Applied Radiation and Isotopes 100 (2015) 21–26

Contents lists available at ScienceDirect

Applied Radiation and Isotopes

journal homepage: www.elsevier.com/locate/apradiso

Study of effective dose of various protocols in equipment cone beam CT

Maria Rosangela Soares [a], Wilson Otto Batista [b,*], Patricia de Lara Antonio [c], Linda V.E. Caldas [c], Ana F. Maia [a]

[a] Federal University of Sergipe, UFS, NPGFI, Rod. Marechal Rondon s/n, Jardim Rosa Elze, CEP: 49.100-000, São Cristóvão, SE, Brazil
[b] Federal Institute of Bahia, IFBA, Rua Emídio dos Santos, s/n. Barbalho, CEP: 40301-015 Salvador, BA, Brazil
[c] Nuclear and Energy Research Institute, IPEN, Av. Lineu Prestes 2242, Cidade Universitária, CEP: 05508-000 São Paulo, SP, Brazil

ARTICLE INFO

Article history:
Received 30 July 2014
Received in revised form
16 December 2014
Accepted 9 January 2015
Available online 10 January 2015

Keywords:
Dental Cone Beam CT
Effective dose
Organs/tissues dose
Thermoluminescent dosimetry

ABSTRACT

This study has the purpose of assessing the radiation absorbed dose in organs/tissues and estimating the effective dose using five different models of Cone Beam Computed Tomography equipment using protocols with similar purpose. For this purpose, 26 thermoluminescent dosimeters were inserted in the position of the organs/tissues of a female anthropomorphic phantom. From the measurements the contribution of $w_T \times H_T$ in the organs and tissues the effective dose were calculated. The measurements have shown the effective dose values within the range 9.3–111.5 μSv. The effective dose values by field of view (FOV) size are within the following ranges: 9.3–51.2 μSv, 17.6–52.0 μSv, and 43.1–111.5 μSv for small/located, medium and large FOV respectively. Protocols with same purpose, carried out with different models of equipment, presented significant differences in the values of the equivalent and effective doses. From the point of view of radiological protection, it is not enough to have knowledge about the dimensions of the FOV and the purpose of the examination. It is necessary to assess the dose using the different models of the equipment and protocols available. In this context, this study provides useful information for this assessment.

1. Introduction

Since the introduction of cone beam computed tomography (CBCT) in dentistry, there has been an increasing use of the technique of CBCT for the various modalities of dental radiological examinations (Koivisto et al., 2012; Pauwels et al., 2012b; Rottke et al., 2013), from the procedures of the planning and the evaluation of dental implants (Qu et al., 2010).

CBCT is an imaging technique that has better three-dimensional spatial resolution and lower absorbed doses to organs/tissues than those results, usually obtained with medical computed tomography in dental applications. After the introduction of CBCT, 3D images have been incorporated into routine dental radiology, and CBCT equipment has gradually replaced other equipment and methods of imaging in dental radiology and in some situations without adequate technical criteria (Morant et al., 2013). However, the advantage presented in terms of the low-dose when compared with conventional computerized tomography for applications in dentistry (Roberts et al., 2009) is not always verifiable when confronted with other modalities in dental radiology, for example, panoramic radiography (Batista et al., 2012).

Currently, a considerable number of models of this equipment are on the market with significant differences in exposure parameters (kV, mA and current-time product), beam quality (filtration), field of view (FOV) and angle rotation. Several studies discuss the absence of uniformity among the various models and the difficulty in implementation of the protocols and guidelines for dosimetric evaluation and quality control (Batista et al., 2013; Koivisto et al., 2012; Pauwels et al., 2012a; Rottke et al., 2013).

Given this variety of equipment, there is some concern among experts in the field of dosimetry and quality control regarding the need to calculate the effective dose in different protocols (Morant et al., 2013) and determine the values of the equivalent dose in the tissue exposed to radiation, such as the thyroid gland (Batista et al., 2013; Pauwels et al., 2012a). In parallel to this need, there are studies which aim to develop phantoms and reproductive methodologies to perform quality control and determine the levels of exposure associated with the various protocols available in the CBCT equipment (Batista et al., 2013).

Simultaneous to these dosimetric studies, usually performed with methodologies already applied to other radiological techniques, there is an effort of researchers to develop specific tools and quality control protocols (Batista et al., 2013; Commission, 2012; Pauwels et al., 2012b; Wu et al., 2014). In 2007 the ICRP 103 (ICRP, 2007) included an explicit weighting factor for salivary glands. In

* Corresponding author.
E-mail address: mrs2206@gmail.com (M.R. Soares).

http://dx.doi.org/10.1016/j.apradiso.2015.01.012
0969-8043/

addition, were introduced new values for the weighting factors including the remainder tissues, the extrathoracic airway and the oral mucosa. These tissues/organs are normally within the field of view (FOV) of the protocols of CBCT. This present study aims to (i) assess the contributions ($w_T \times H_T$) of the tissues/organs from different models of CBCT equipment with protocols having the same purpose and, consequently, (ii) to estimate the effective dose of five different models of CBCT equipment which present differences in their fundamental parameters.

2. Materials and methods

2.1. Anthropomorphic phantom

In this study, a female Alderson anthropomorphic phantom manufactured by Radiology Support Devices™ was used. The phantom represents a typical adult woman 1.6 m in height and 55 kg in weight (Goren et al., 2013). It consists of an original human skeleton filled with material of atomic mass equivalent to human soft tissues. Ten slices with a thickness of 2.5 cm, as shown in Fig. 1, were used. The slices had various cylindrical holes filled with rods. Each rod had an appropriate space, 3 mm × 3 mm × 1 mm, for the placement of the dosimeters.

2.2. Equipment CBCT and protocols

For this study were evaluated nine 3D image acquisition protocols in five different pieces of equipment. The models of the CBCT equipment and the protocols evaluated are presented in Table 1. For all protocols, exposures were carried out in an anthropomorphic phantom, with the same conditions of a real patient (technical and geometric parameters). The X-ray emission pulsed mode was used for all protocols. The protocols used in the facility images were evaluated for each model and classified according to the dimensions of the field of view (FOV) and purpose of the examination as follows: (i) large FOV, protocols with a diameter greater than 14 cm (Gendex and i-CAT), which scan both jaws in a single exposure; (ii) small FOV, localized protocol, for the images of some dental units; (iii) 1 arch protocols, protocols for the full arch images (in this study, the upper jaw) in a single exposure and (iv) two-arch protocols (8 cm of height), protocols that scan both jaws in a single exposure. The technical parameters of the selected protocols are present in Table 1.

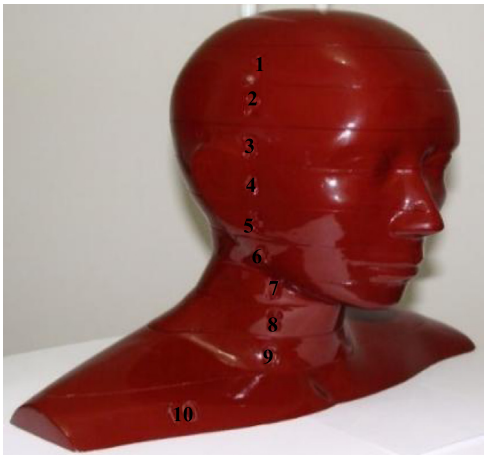

Fig. 1. Head and neck of the anthropomorphic phantom representing a typical adult woman.

2.3. Thermoluminescent dosimeters

Twenty-six thermoluminescent dosimeters were used (*TLD-100* consisting of *LiF: Mg, Ti*). The TLDs were calibrated at known values of exposure, ranging from 1 to 15 mGy, in diagnostic radiology qualities, with computed tomography protocols RQT8, RQT9 and RQT10. Industrial x-ray equipment was used for this calibration: a *Pantak/Seifert 160HS ISOVOLT* property of the *Institute of Nuclear Energy Research (IPEN)* in São Paulo, Brazil. All readings (calibration and measurements) were performed on a *Harshaw TLD reader*, model *QS 3500*™, with the aid of *WinREMS*™ software coupled to a data acquisition system. The dose response curve was determined from the calibration with a coefficient of variation of 8%. The measurement of the dose was determined in each TLD because of the dose–response curves, presented in Fig. 2, corrected by the calibration factor of the dosimeter and the reference light at the time of reading. The result had the maximum uncertainty of the order of 10%.

2.4. Positioning of the TLD in the phantom

The selection of tissues and organs was based on the methodology described and presented by Ludlow et al. (2006) and Roberts et al. (2009). The organs and tissues, radiosensitively selected, in the FOV, are defined in the last recommendation published by the International Commission on Radiological Protection, ICRP 103 (ICRP, 2007). In all of the, eight relevant organs and/or tissues, within or close to the radiation field, were selected for evaluation: thyroid, esophagus, brain, skin, salivary glands, bone marrow, bone surface and remainder tissues. For organs and tissues partly included, the following percentages have been considered: 10% for the fraction of radiation in the esophagus, 5% for the fraction in the total body skin on the skin surface area in the head and neck area and 5% for the proportion of radiation in lymphatic nodes and muscles in the head and neck area of the total body mass (Koivisto et al., 2012; Ludlow et al., 2003).

For the location of the tissues and organs, the support of an oral radiologist was enlisted. In each protocol, three exposures were carried out and the response of the dosimeter was divided by three. The positions of the dosimeters in slices of the phantom are presented in Table 2.

2.5. Equivalent dose, H_T

For the determination of the organ or tissue equivalent dose, H_T , the following equation was used:

$$H_T = w_R \times \sum_i f_i \times D_{Ti} \quad (1)$$

Here, w_R is the radiation weighting factor (w_R=1 Sv/Gy for X-rays), f_i is the mass fraction of the tissue T_i in the slice i that has been irradiated, and D_{Ti} is the average absorbed dose in the fraction of tissue/organ T contained in slice i as presented in Table 3 (Koivisto et al., 2012; Roberts et al., 2009).

The equivalent dose in the salivary glands, bone marrow and bone surface was calculated by averaging the equivalent dose of the tissues and organs corresponding those organs. For the other organs and tissues was utilized direct reading of the dosimeter.

2.6. Effective dose, E

The calculation of the effective dose on a large number of organs and tissues is based on ICRP, 2007. Some organs and tissues are explicitly listed, and others classified are remainder tissues.

To calculate the effective dose E, the sum of the products of H_T by the weighting factor for the corresponding tissue w_T was

Table 1
Technical parameters of the selected protocols in CBCT.

CBCT		Protocol	FOV[a] (cm²)	kV	mA	mAs	rotation arc (deg)	Filtration[b]
Manufacturer	**Model**							(mm) Al
Planmeca	ProMax™ 3D	Localized[c]	5 × 8	84	12	144	200	22
Gendex	GXCB 500™	Large FOV	14 × 8.5	120	5	46.5	360	16.7
		2 arch	8.5 × 8.5	120	5	46.5	360	16.7
		1 arch[d]	8.5 × 6	120	5	46.5	360	16.7
Imaging sciences	i-CAT Classical™	Large FOV	16 × 8	120	3–7	36.2	360	14
		1 arch[d]	16 × 6	120	3–7	36.2	360	14
Sirona	Orthophos XG™ 3D	Localized[c]	5 × 5	85	7	42.6	180	14
		2 arch	8 × 8	85	7	42.6	180	14
Carestream health	CS 9000™	Localized[c]	5 × 3.7	70	8	92.2	360	3.2

[a] Diameter × height.
[b] Measured values.
[c] Upper jaw in the anterior region.
[d] Upper jaw.

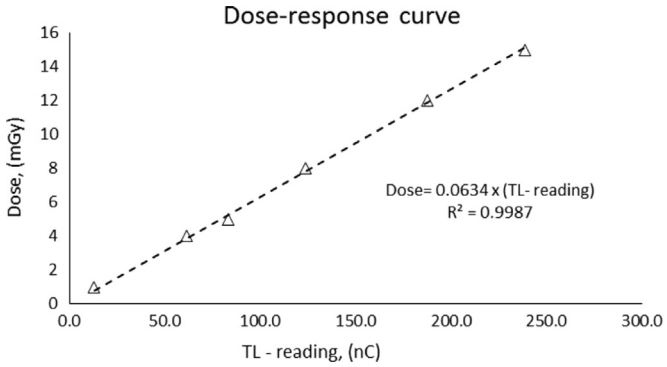

Fig. 2. Dose response curve for the range from 1 to 15 mGy.

Table 2
Location of the TLDs in the phantom.

No TLD	Organ (slice)
1	Surface of the left side (5)*
2	Posterior neck (5)*
3	Left thyroid (8)*
4	Right lens (3)*
5	Left lens (3)*
6	Posterior calvarium (2)
7	Calvarium right (2)
8	Calvarium left (2)
9	Anterior calvarium (2)
10	Middle point of the brain (2)
11	Pituitary gland (3)
12	Right orbit (3)
13	Left orbit (3)
14	Center of the spinal column (5)
15	Right parotid (5)
16	Right branch (5)
17	Left parotid (5)
18	Left branch (5)
19	Center of the sublingual gland (6)
20	Right submandibular (6)
21	Left submandibular (6)
22	Right mandible (6)
23	Left mandible (6)
24	Esophagus (9)
25	Right thyroid (9)
26	Left thyroid (9)

* TLDs placed on the surface.

carried out

$$E = \sum_T H_T \times w_T \quad (2)$$

Table 3
ICRP 103 (ICRP, 2007) Weighting factor tissue, w_T; fraction irradiated, f_i; and dosimeters used to calculate the effective dose.

Organ/tissue	Weighting factor (w_T)	f_i	Dosimeter
Bone marrow	0.12	0.165	
Calvaria		0.118	6, 7, 8, 9, 12, 13
Center of the spinal column		0.034	14
Mandible		0.012	16, 18, 22, 23
Eosophagus	0.04	0.1	24
Thyroid	0.04	1	3, 25, 26
Skin	0.01	0.05	1, 2, 3, 4
Bone surface[a]	0.01	0.165	
Brain	0.01	1	9, 10
Salivary glands	0.01	1	
Parotid			15, 17
Submandibular			20, 21
Sublingual gland			19
Remaining tissues	0.12		
Lymphatic nodes		0.05	15, 17, 19, 20, 21
Extrathoracic airway		1	12,13, 15, 17, 24, 25, 26
Muscle		0.05	15, 17, 19, 20, 21
Oral mucosa		1	16, 15, 17, 18, 19, 20, 21, 22, 23

[a] Bone surface dose = Bone marrow dose × 3.23.

For the dosimetric evaluation for the remainder tissues, those were selected for tissues that were within or close to the radiation field, which is relevant for this evaluation. For these tissues, the effective dose was calculated from the using the product of weighting factor for remainder tissues by value of equivalent doses divided by total number of remainder organs. The weighting factors, w_T, for the tissues and organs were defined by ICRP 103(ICRP, 2007) as described in Table 3.

3. Results

The results of equivalent doses determined in the tissues studied are presented in Table 4 together with the effective doses. Table 4 also presents that the doses range from 10.5 μSv to 111.5 μSv for the different protocols in this study.

Fig. 3 compares the results of the protocols of large FOV (Gendex and i-CAT equipment) by using comparable FOV diameters.

Fig. 4 presents the results for the equivalent doses associated with the localized protocol. Other comparisons are made in Figs. 5 and 6, for the one-arch and two-arch protocols respectively.

Table 4
Effective dose (μSv), the contributions ($w_T \times H_T$) of various organ doses to the effective dose and the relative value of the contribution of the dose to each organ/tissue studied in relation to the effective dose.

	ProMax 3D		Gendex GXCB		i-CAT classical		Orthophos XG 3D		CS 9000
Protocol	Localized	Large FOV	2-arch	1-arch	Large FOV	1-arch	Localized	2-arch	Localized
Salivary glands	**20.0 (29%)**	**11.2 (26%)**	**15.5 (30%)**	**14.6 (28%)**	**27.9 (25%)**	**16.0 (26%)**	**2.9 (27%)**	**5.4 (33%)**	**4.5 (49%)**
Thyroid	**6.8 (10%)**	**6.1 (14%)**	**6.4 (12%)**	**7.7 (15%)**	**19.9 (18%)**	**6.7 (11%)**	**0.8 (7.5%)**	**2.8 (16%)**	**0.8 (8.6%)**
Bone marrow	**8.7 (13%)**	**6.5 (15%)**	**6.5 (13%)**	**6.1 (12%)**	**15.7 (14%)**	**12.4 (20%)**	**1.7 (16%)**	**1.6 (7.1%)**	**0.6 (6.5%)**
Bone surface	**2.3 (3.3%)**	**1.7 (3.9%)**	**1.8 (3.5%)**	**1.7 (3.6%)**	**4.2 (4%)**	**3.3 (5.3%)**	**0.5 (4.7%)**	**0.4 (1.4%)**	**0.2 (2.2%)**
Esophagus	**0.8 (1.2%)**	**0.6 (1.4%)**	**0.6 (1.2%)**	**0.8 (1.6%)**	**2.1 (1.9%)**	**0.6 (1.2%)**	**0.1 (1.0%)**	**0.3 (1.4%)**	–
Brain	**1.7 (2.5%)**	**1.3 (3.0%)**	**1.2 (2.3%)**	**0.9 (2%)**	**2.6 (2.3%)**	**2.5 (4.3%)**	**0.2 (1.9%)**	**0.2 (1.4%)**	–
Skin	**0.9 (1.3%)**	**0.3 (0.7%)**	**0.6 (1.2%)**	**0.4 (0.8%)**	**0.9 (0.8%)**	**0.7 (1.2%)**	**0.2 (1.9%)**	**0.3 (1.4%)**	**0.3 (3.2%)**
Remainder	**27.1 (40%)**	**15.3 (36%)**	**19.4 (37%)**	**18.9 (37%)**	**38.3 (34%)**	**20.4 (32%)**	**4.2 (40%)**	**6.6 (38%)**	**2.8 (30%)**
Effective dose (ICRP 103)	68.3	43.1	52.0	51.2	111.5	62.7	10.5	17.6	9.3

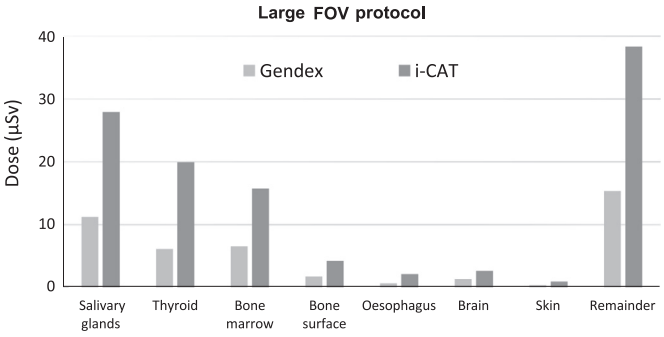

Fig. 3. Comparison of the dose by various organs/tissues for the large FOV protocol.

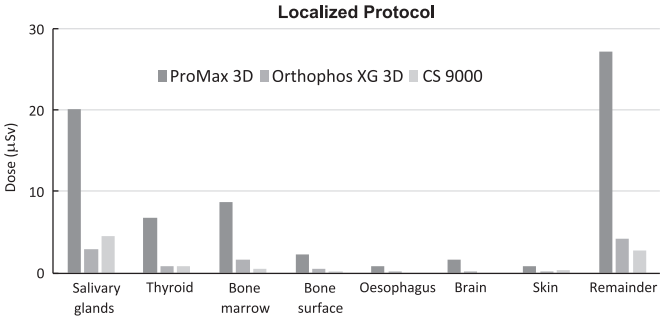

Fig. 4. Comparison of the dose by various organs/tissues for the localized protocol.

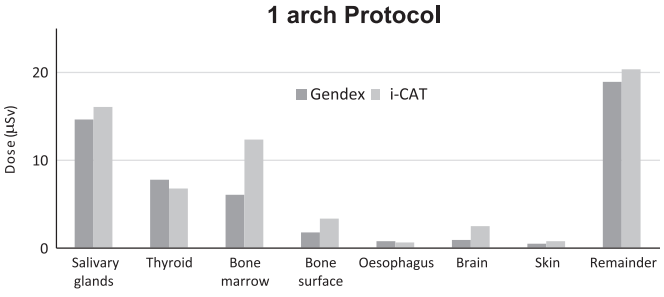

Fig. 5. Values for the equivalent dose in tissues/organs studied for the 1-arch protocol.

Table 4 shows the values of the individual contributions of the organs/tissues to the effective dose obtained in each protocol.

4. Discussion

This study estimated the effective dose for five different models of dental CBCT equipment for the various FOV, usually used in clinical radiological procedures. It also evaluated the equivalent dose in eight different organs/tissues.

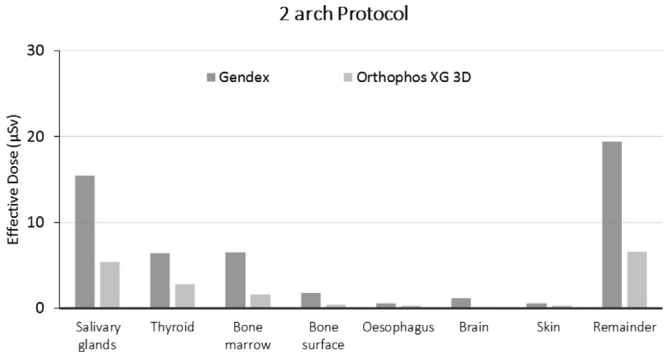

Fig. 6. Values for the equivalent dose in tissues/organs studied the for 2-arch protocol.

To compare the results obtained in this study, with the results from other studies, one must consider the particular phantom used and the placement of the dosimeters in each case (Pauwels et al., 2012a; Qu et al., 2010). In this study, a female phantom was used. The knowledge obtained from our study contributes for the estimation of the effective dose in women and also in evaluating the individual contributions to the contribution of $w_T \times H_T$ of the tissues within the radiation field or close to it. Morant et al. (2013) in their studies have shown that the equivalent dose in the center of the brain is very close in males and females. In other tissues, however because of the dimensions of the phantom, the equivalent dose is higher in the organs/tissues of a female phantom (Morant et al., 2013).

The ProMax 3D™ CBCT for the FOV of 5 cm × 8 cm (diameter × height) presented an estimated effective dose of 68.3 μSv. For this same equipment, there are data of other authors, as shown in Table 5. The comparison of our results with the other investigations showed in Table 5, there exist significant differences, due to the differences in the dimensions of FOV. It is worth mentioning that the results presented in other studies also present a great variation in the final results for the effective dose. Although the FOV dimensions used in this study are slightly different from other studies, a great range of results for different works with similar protocols was observed.

For the CS 9000 3D™ CBCT equipment for the 5 cm × 3.7 cm (diameter × height) FOV, the old Kodak 9000™, with a localized protocol presented an effective dose of 17.6 μSv. In two other relevant studies, the authors found the following values for the effective dose: 19 μSv (Pauwels et al., 2012a) and 24 μSv (Theodorakou et al., 2012) as shown in Table 6. This difference can be related to the exposure parameters (mAs) used and the FOV location, but our results are coherent with these studies.

Table 5
Values of the effective doses from the present study and the results available in the literature for the ProMax 3D equipment.

Other study	Dose range	Present study
(Rottke et al., 2013)	23 μSv (84 kV; FOV 3.2 cm × 4.2 cm; 1 mA)	
	357 μSv (84 kV; FOV 8 cm × 8 cm; 16 mA)	68.3 μSv
(Pauwels et al., 2012a)	28 μSv (84 kV; FOV 8 cm × 8 cm; 19.9 mAs)	84 kV
	122 μSv (84 kV; FOV 8 cm × 8 cm; 169 mAs)	FOV 5 cm × 8 cm
(Koivisto et al., 2012)	153 μSv – MOSFET (84 kV; FOV 8 cm × 8 cm; 145 mAs)	12 mA
	131 μSv – Monte Carlo	144 mAs
(Qu et al., 2010)	216 μSv (84 kV; FOV 8 cm × 8 cm; 144 mAs)	

Table 6
Comparison of the values of the effective doses from the present study and the results available in the literature for the CS 9000 equipment.

Other study	Dose range	Present study
(Pauwels et al., 2012a)	19 μSv (70 kV; 107 mAs)	17.6 μSv 88.41 mAs
(Theodorakou et al., 2012)	24 μSv (70 kV; 106.8 mAs) young phantom	8 mA 70 kV

The value associated with the equipment i-CAT™, using the protocol of large FOV is 111.5 μSv. This result can be compared with the studies of Loubele et al. (2009) and Ludlow et al. (2006), as shown in Table 7. In this comparison, it is observed that our result is consistent with the values published by these authors.

For the localized protocol, the Orthophos XG™ 3D equipment was the one with the lowest effective dose, 10.5 μSv, when compared with similar protocols for other types of equipment such as of the ProMax™ 3D (68.3 μSv) and CS 9000 (9.3 μSv). Specifically, the effective dose derived from the ProMax™ 3D equipment (FOV = 5.0 cm × 8.0 cm) was more than six times the effective dose values obtained with the Orthophos XG™ 3D equipment (FOV = 5.0 cm × 5.0 cm) and CS 9000™ 3D (FOV = 5.0 cm × 3.7 cm). In this comparison, even considering the height of the FOV in ProMax™ 3D equipment is capable of acquiring image of dental units of two arcades (upper and lower). But still, it is not reasonably to have the high difference in the effective dose. Certainly, the differences are associated with technical parameters (kV, mAs, filtration and others) and geometrical parameters. These differences in the effective dose among the types of equipment are confirmed in evaluating the contributions ($w_T \times H_T$) of the tissues/organs, as shown in Fig. 4 where the protocol used by the ProMax™ 3D equipment has the highest value in all tissue and organs.

When the evaluation of large FOV protocol, was carried out, a difference between the Gendex and i-CAT equipment is observed. The protocol 14 cm × 8.5 cm of the Gendex equipment produces an image with 14 cm in diameter with dimension of radiation field equal to ~8 cm × 8.5 cm by turning off-axis. The significant difference in the value of effective dose can be explained through the contributions $w_T \times H_T$ of tissues and organs as shown in Fig. 3.

Table 7
Comparison of the values of the effective doses from the present study and the results available in the literature for the i-CAT equipment.

Other study	Dose range	Present study
(Loubele et al., 2009)	77 μSv (120 kV; 3–8 mA, 39.5 mAs) FOV 13 cm × 6 cm)	111.5 μSv 36.2 mAs
(Ludlow et al., 2006)	135 μSv (120 kV; 10 mA, 37.3 mAs full FOV)	3–7 mA 120 kV

For the evaluation of the protocols of 2 dental arches, as it can be observed in Table 4, that the Gendex equipment presents an effective dose of more than three times the value of the effective dose of the Orthophos™ equipment. Even when the size of the FOV of both equipment is comparable, the arc of rotation, filtration and kV are determinants that explain the difference, shown in Table 1.

Especially for the protocols with FOV of a single dental arcade the upper jaw, in this study, the effective doses for both types of equipment tested were: 51.2 μSv (Gendex GXCB 500™) and 62.7 μSv (i-CAT Classical™). This difference corresponds to 18%, a value not being significant. The values of the contributions of $w_T \times H_T$ for tissues and organs are shown in Fig. 5, indicating only a significant difference in the bone marrow.

In assessing the contribution of the tissues/organs for the effective dose, presented in Table 4, it was observed that, individually, the salivary glands contributed around approximately 30%. The remainder tissues have the largest contribution, an average of 36% of the calculated effective dose. These results are in accordance with studies conducted by Pauwels et al. (2012a,b), Koivisto et al. (2012) and Roberts et al. (2009), where the remainder tissues were those having the greatest contribution to the effective dose, followed by the salivary glands. It is noteworthy that the salivary glands were included as an organ individually listed, from the publication of ICRP 103 (ICRP, 2007). This implies a significant contribution to the effective dose, compared to previous studies before the publication of ICRP 103.

CS 9000 equipment had the highest contribution of $w_T \times H_T$ in the salivary glands, 48% of the effective dose, 9.3 μSv. Even though a low value when compared with other protocols, it should be considered that, this equipment has the smaller FOV of 3.7 cm × 5 cm. When this value is compared with the Orthophos™ with a FOV of 5 cm × 5 cm for, protocol, the estimation of the effective dose is 10.5 μSv, with an equivalent dose of the salivary glands of 2.9 μSv, corresponding to 27% of the effective dose value.

The thyroid and bone marrow also present a significant contribution to the effective dose values. The contributions of the skin, brain, bone surface and esophagus were individually insignificant.

These results should be interpreted on the basis of clinical purpose and the aspects of radiological protection, considering the dimensions of the FOV, the geometric parameters, and the exposure parameters (kV, mA and the waveform – continuous or pulsed x-ray beam). Another aspect that reinforces this need is to be aware that different protocols with the same diagnostic purposes lead to different values of the equivalent dose in organs/tissues. This whole analysis confirms the need for studies that estimate the contribution of the tissues/organs to the effective dose and the effective dose in the various models of equipment available on the market.

The results suggest the need of assessing the dose in tissues and organs, especially the salivary glands and remainder tissue that contribute more than 60% of the effective dose.

In the analysis of the possible limitations associated with this study, the following conclusions can be realised: (i) the limited number of dosimeters, (26 TLD); (ii) uncertainties of the order of 10% and (iii) the phantom female. However, the uncertainties and the number of dosimeters are typical in this type of evaluation. The use of a female phantom is a certain contribution for generating data of effective dose for women, teens and person with low bodyweight.

5. Conclusions

This study presents effective dose values associated with different protocols and different types of equipment. The authors

conclude that the differences in the dose values, even when the protocols have the same purpose, are due to a lack of uniformity in the essential exposure parameters of acquired image. Thus from the point of view of radiological protection, it is not enough to know the dimensions of the field of vision and the purpose of the examination. It is necessary to assess the dose of the different models of equipment and available protocols.

Simultaneous to these dosimetric studies, usually performed with methodologies already applied to other radiological techniques, there is an effort of researchers to develop specific tools and quality control protocols (Batista et al., 2013; Commission, 2012; Pauwels et al., 2012b; Wu et al., 2014). In 2007 the ICRP 103 (ICRP, 2007) included an explicit weighting factor for salivary glands. In addition, were introduced new values for the weighting factors including the remainder tissues, the extrathoracic airway and the oral mucosa. These tissues/organs are normally within the field of view (FOV) of the protocols of CBCT. This present study aims to (i) assess the contributions ($w_T \times H_T$) of the tissues/organs from different models of CBCT equipment with protocols having the same purpose and, consequently, (ii) to estimate the effective dose of five different models of CBCT equipment which present differences in their fundamental parameters, without limiting the ability of the manufacturers for new innovations. In this context, the present study provides useful information for this type of analysis. Also, it contributes to the implementation of optimization practices and the appropriate choice of image protocol that best suits the diagnostic needs.

Acknowledgements

The authors thank the Laboratory of Physical Radiology of the Federal Institute of Bahia (LAFIR/IFBA) and the Institute of Nuclear Energy Research Lab (IPEN).

References

Batista, W.O., Navarro, M.V., Maia, A.F., 2012. Effective doses in panoramic images from conventional and CBCT equipment. Radiat. Prot. Dosim. 151, 67–75.
Batista, W.O., Navarro, M.V., Maia, A.F., 2013. Development of a phantom and a methodology for evaluation of depth kerma and kerma index for dental cone beam computed tomography. Radiat. Prot. Dosim. 157, 543–551.
Commission, European, 2012. Cone beam CT for dental and maxillofacial radiology. European Commission, Luxembourg, p. 154, Radiation Protection no 172.
Goren, A.D., Prins, R.D., Dauer, L.T., Quinn, B., Al-Najjar, A., Faber, R.D., Patchell, G., Branets, I., Colosi, D.C., 2013. Effect of leaded glasses and thyroid shielding on cone beam CT radiation dose in an adult female phantom. Dentomaxillofac. Radiol. 42, 20120260.
ICRP, 2007. The 2007 recommendations of the international commission on radiological protection. ICRP publication 103. Ann. ICRP, 1–332 (12/18 ed).
Koivisto, J., Kiljunen, T., Tapiovaara, M., Wolff, J., Kortesniemi, M., 2012. Assessment of radiation exposure in dental cone-beam computerized tomography with the use of metal-oxide semiconductor field-effect transistor (MOSFET) dosimeters and Monte Carlo simulations. Oral Surg. Oral Med. Oral Pathol. Oral Radiol. 114, 393–400.
Loubele, M., Bogaerts, R., Van Dijck, E., Pauwels, R., Vanheusden, S., Suetens, P., Marchal, G., Sanderink, G., Jacobs, R., 2009. Comparison between effective radiation dose of CBCT and MSCT scanners for dentomaxillofacial applications. Eur. J. Radiol. 71, 461–468.
Ludlow, J., Davies-Ludlow, L., Brooks, S., 2003. Dosimetry of two extraoral direct digital imaging devices: NewTom cone beam CT and orthophos plus DS panoramic unit. Dentomaxillofac. Radiol. 32, 229–234.
Ludlow, J.B., Davies-Ludlow, L.E., Brooks, S.L., Howerton, W.B., 2006. Dosimetry of 3 CBCT devices for oral and maxillofacial radiology: CB mercuray, NewTom 3G and i-CAT. Dentomaxillofac. Radiol. 35, 219–226.
Morant, J., Salvadó, M., Hernández-Girón, I., Casanovas, R., Ortega, R., Calzado, A., 2013. Dosimetry of a cone beam CT device for oral and maxillofacial radiology using Monte Carlo techniques and ICRP adult reference computational phantoms. Dentomaxillofac. Radiol. 42, 92555893.
Pauwels, R., Beinsberger, J., Collaert, B., Theodorakou, C., Rogers, J., Walker, A., Cockmartin, L., Bosmans, H., Jacobs, R., Bogaerts, R., Horner, K., 2012a. Effective dose range for dental cone beam computed tomography scanners. Eur. J. Radiol. 81, 267–271.
Pauwels, R., Theodorakou, C., Walker, A., Bosmans, H., Jacobs, R., Horner, K., Bogaerts, R., Consortium, S.P., 2012b. Dose distribution for dental cone beam CT and its implication for defining a dose index. Dentomaxillofac. Radiol. 41, 583–593.
Qu, X.M., Li, G., Ludlow, J.B., Zhang, Z.Y., Ma, X.C., 2010. Effective radiation dose of ProMax 3D cone-beam computerized tomography scanner with different dental protocols. Oral Surg. Oral Med. Oral Pathol. Oral Radiol. Endod. 110, 770–776.
Roberts, J.A., Drage, N.A., Davies, J., Thomas, D.W., 2009. Effective dose from cone beam CT examinations in dentistry. Br. J. Radiol. 82, 35–40.
Rottke, D., Patzelt, S., Poxleitner, P., Schulze, D., 2013. Effective dose span of ten different cone beam CT devices. Dentomaxillofac. Radiol. 42, 20120417.
Theodorakou, C., Walker, A., Horner, K., Pauwels, R., Bogaerts, R., Jacobs, R., 2012. Estimation of paediatric organ and effective doses from dental cone beam CT using anthropomorphic phantoms. Br. J. Radiol. 85, 153–160.
Wu, J., Shih, C.-T., Ho, C.-h, Liu, Y.-L., Chang, Y.-J., Min Chao, M., Hsu, J.-T., 2014. Radiation dose evaluation of dental cone beam computed tomography using an anthropomorphic adult head phantom. Radiat. Phys. Chem. 104, 287–291.